Fermi velocity renormalization and the excitonic insulator in graphene

Joaquín E. Drut[1] and Timo A. Lähde[2]

[1]*Department of Physics and Astronomy, University of North Carolina, Chapel Hill, North Carolina 27599-3255, USA*
[2]*Institut für Kernphysik, Institute for Advanced Simulation, and Jülich Center for Hadron Physics, Forschungszentrum Jülich, D-52425 Jülich, Germany*

We compute the Fermi velocity of the Dirac quasiparticles in clean graphene at the charge neutrality point for strong Coulomb coupling α_g. We perform a Lattice Monte Carlo calculation within the low-energy Dirac theory, which includes an instantaneous, long-range Coulomb interaction. This method is non-perturbative and takes full account of quantum fluctuations. We find a finite renormalized Fermi velocity $v_{FR} > v_F$, where $v_F \simeq c/300$. We introduce the critical Fermi velocity renormalization $v_c \equiv v_{FR}(\alpha_{gc})/v_F$, where α_{gc} is the critical coupling for the semimetal-insulator transition due to excitonic pair formation. We compare our results with empirical studies of interaction-induced spectral changes in graphene. We find $v_c \simeq 3.3$, which should be contrasted with $v_{FR}/v_F \simeq 2-3$ for ultra-clean suspended graphene and $v_{FR}/v_F \simeq 1.2$ for graphene on a boron nitride substrate. Our results are consistent with the non-observation of insulating states in suspended graphene in the absence of an external magnetic field. We also discuss the dynamical critical exponent z.

PACS numbers: 73.63.Bd, 05.10.Ln, 71.30+h

Graphene, a two-dimensional membrane of carbon atoms with unique electronic properties, is characterized by a low-energy spectrum of Dirac quasiparticles, with a Fermi velocity $v_F \simeq 1/300$ of the speed of light in vacuum [1, 2]. As the strength of the Coulomb interaction between the quasiparticles is controlled by $\alpha_g \equiv e^2/(4\pi\epsilon v_F) \simeq 2.2/\epsilon$, the role of interactions can be enhanced to the point that graphene may resemble Quantum Electrodynamics (QED) in a strongly coupled regime [3]. In particular, the unscreened, long-range Coulomb interaction in graphene leads to non-trivial velocity renormalization effects. These have been extensively analyzed in the weak-coupling regime [4], and at strong coupling in the random-phase approximation [5, 6]. At weak coupling, a logarithmic running $v_F(n)/v_F(n_0) = 1 + (\alpha_g/4)\ln(n_0/n)$ with carrier density n is found, thus the renormalized Fermi velocity v_{FR} is expected to become large in the vicinity of the Dirac point ($n = 0$). On the experimental side, logarithmic velocity renormalization has been detected in ultra-clean suspended graphene [7], on boron nitride (BN) substrates [8], and in ARPES measurements of quasi-freestanding graphene on silicon carbide (SiC) [9]. These experiments find $v_{FR}/v_F > 1$ at the Dirac point, with the largest renormalization $v_{FR}/v_F \simeq 2-3$ in suspended graphene, where $\epsilon = 1$.

In addition to the renormalization of v_F, strong electron-electron interactions may trigger a semimetal-insulator transition due to the excitonic pairing of quasiparticles and holes above a critical coupling α_{gc}. Notably, spontaneous gap generation in graphene has been studied using the Schwinger-Dyson (or gap) equations [10], and within the Lattice Monte Carlo (LMC) framework, which is non-perturbative and takes full account of quantum fluctuations. In particular, LMC is noted for its central role in the study of dynamical mass generation (or spontaneous chiral symmetry breaking) in gauge field theories, such as QED and Quantum Chromodynamics (QCD), see Ref. [11] and references therein. In the case of graphene, LMC has been applied to the Dirac theory using a contact interaction related to the Thirring model [12], a long-range Coulomb interaction [13, 14], and to the tight-binding description using a Hubbard interaction [15]. The LMC calculation of Ref. [13] found $\alpha_{gc} \simeq 1.11 \pm 0.06$, which suggests that the insulating phase might be observable in ultra-clean suspended graphene samples, as $\alpha_{gc} < 2.2$. So far, the semimetal-insulator transition has not been detected, although the observed $v_{FR}/v_F \simeq 2-3$ in suspended graphene is indicative of interaction-induced spectral changes [3, 7].

Our objective is to compute $v_{FR}(\alpha_g)/v_F$ at the Dirac point, and to contrast this with the electronic phase diagram. Specifically, we shall consider the "critical velocity renormalization" $v_c \equiv v_{FR}(\alpha_{gc})/v_F$, *i.e.* the velocity renormalization at the critical coupling α_{gc}. Then, the semimetal-insulator transition should only be observable when the velocity renormalization exceeds v_c for $n = 0$. A clear advantage of v_c over α_{gc} is that the former is a renormalized (physical) quantity which can be directly compared with a wide range of experiments.

The LMC treatment of graphene uses the linearized low-energy Hamiltonian [16, 17] with an instantaneous Coulomb interaction. This gives the Euclidean (continuum) action

$$S_E = \frac{1}{2g^2}\int d^3x\, dt\, (\partial_t A_0)^2 + \sum_{a=1}^{N_f}\int d^2x\, dt\, \bar{\psi}_a D[A_0]\psi_a, \tag{1}$$

where $g^2 \equiv e^2/\epsilon$ with $\epsilon = (1+\kappa)/2$ for a substrate with dielectric constant κ, ψ_a is a four-component Dirac field in $2+1$ dimensions with $\bar{\psi} \equiv \psi^\dagger\gamma_0$, A_0 is the gauge (photon) field in $3+1$ dimensions, and $N_f = 2$ for a graphene monolayer. The Dirac operator is

$$D[A_0] = \gamma_0(\partial_0 + iA_0) + v_F\sum_{k=1}^{2}\gamma_k\partial_k + m_0, \tag{2}$$

where the Dirac matrices γ_μ satisfy the Euclidean Clifford algebra $\{\gamma_\mu, \gamma_\nu\} = 2\delta_{\mu\nu}$, and m_0 is the bare fermion mass, which provides an infrared regulator for modes that would otherwise be massless when the U($2N_f$) chiral symmetry of Eq. (1) is spontaneously broken.

The lattice version of Eq. (1) is preferably formulated in terms of "staggered" fermions [18], *i.e.* one-component Grassmann variables $\chi, \bar{\chi}$, which partially retain the U($2N_f$) chiral symmetry of Eq. (1) at finite lattice spacing. The full symmetry is recovered in the continuum limit. Every other lattice site in the staggered formulation is identified with a space-time degree of freedom, and the resulting "hypercubes" of lattice sites are treated as internal degrees of freedom. The four-component Dirac spinors are reconstructed in the continuum limit as appropriately chosen combinations of the staggered fermions in each hypercube. Staggered fermions have been successfully applied to theories ranging from QED$_3$ [19] and QED$_4$ [20–22] to the Thirring model [23, 24]. In QCD, staggered fermions have been developed into highly improved lattice actions, which systematically remove the discretization errors, see Ref. [11] for an overview. The application of staggered fermions to Eq. (1) is detailed in Ref. [13], and a pedagogical introduction can be found in Ref. [25].

The fermionic part of Eq. (1) is given for $N_f = 2$ in terms of staggered fermions as $\sum_{\mathbf{n},\mathbf{m}} \bar{\chi}_{\mathbf{n}} K_{\mathbf{n},\mathbf{m}}[\theta_0] \chi_{\mathbf{m}}$, where $\mathbf{n} \equiv (n_0, n_1, n_2) = (t, x, y)$ and $\mathbf{m}$ denote lattice sites on a $2+1$ dimensional fermion brane. The staggered Dirac operator is

$$K_{\mathbf{n},\mathbf{m}}[\theta_0] = \frac{1}{2a}(\delta_{\mathbf{n}+\mathbf{e}_0,\mathbf{m}}\, U_{0,\mathbf{n}} - \delta_{\mathbf{n}-\mathbf{e}_0,\mathbf{m}}\, U^\dagger_{0,\mathbf{m}}) + \frac{\lambda}{2a}\sum_i \eta^i_{\mathbf{n}}(\delta_{\mathbf{n}+\mathbf{e}_i,\mathbf{m}} - \delta_{\mathbf{n}-\mathbf{e}_i,\mathbf{m}}) + m_0\,\delta_{\mathbf{n},\mathbf{m}}, \quad (3)$$

where $\eta^1_{\mathbf{n}} = (-1)^{n_0}$, $\eta^2_{\mathbf{n}} = (-1)^{n_0+n_1}$, with $\mathbf{e}_i$ a unit vector in lattice direction i. The invariance of Eq. (1) under spatially uniform, time-dependent gauge transformations is retained by coupling the fermions to the lattice gauge field θ_0 via "gauge links" $U_0 \equiv \exp(i\theta_0)$. Our LMC calculations are performed for $v_F = 1$ (thus $g^2 \to g^2/v_F$) and we take $a/a_x = 1$, where $a \equiv a_t$ is the temporal lattice spacing, and therefore $\lambda = 1$. However, at non-zero α_g we have $\lambda_R \equiv v_{FR}\,(a/a_x)_R$, from which the velocity renormalization v_{FR}/v_F can be obtained once the lattice spacing asymmetry $(a/a_x)_R$ is known. We emphasize that our cubic space-time lattice should not be understood in terms of a square tight-binding theory. The low-energy physics of graphene described by Eq. (1) is recovered in the continuum limit $a \to 0$, taken along lines of constant physics (as a function of the bare parameters) in the direction of increasing correlation length [13, 21].

We compute the renormalized λ_R and m_R from the staggered fermion propagator

$$C_f(t,x,y) \equiv \langle \chi(t,x,y)\bar{\chi}(t_0,x_0,y_0)\rangle = \langle K^{-1}_{\mathbf{n},\mathbf{n}_0}\rangle, \quad (4)$$

on an $N_x^2 \times N_t$ space-time lattice with $N_{x,t}/4$ integer. Here $\mathbf{n}_0$ is an arbitrary point of reference, and the brackets denote an average over "ensembles" of gauge field configurations, obtained as a function of $\beta \equiv v_F/g^2 = 1/(4\pi\alpha_g)$ and m_0 with the Hybrid Monte Carlo (HMC) algorithm [26]. Once $C_f(t,x,y)$ is computed, we form the temporal correlator

$$C_{ft}(t,p_1,p_2) \equiv \sum_{x,y} \exp(-ip\cdot x)\, C_f(t,x,y), \quad (5)$$

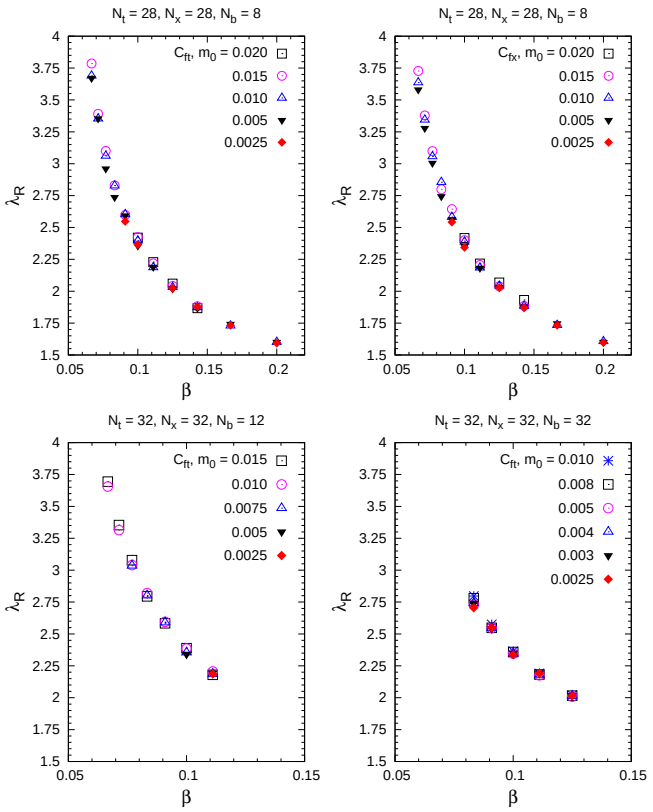

FIG. 1: Calculation of λ_R as a function of $\beta = 1/(4\pi\alpha_g)$ and m_0 from the correlators C_{ft} and C_{fx} on different lattices. Statistical errors are comparable to the size of the symbols.

for momenta $p_i = 2\pi n/N_x$, with $n = -N_x/4, \ldots, N_x/4$, timeslices $t = 0, \ldots, N_t - 1$, and summation over even lattice sites, defined by $(-1)^{t+x+y} = 1$. The temporal correlator C^R_{ft} with renormalized m_R and λ_R has been given in Ref. [21]. The expression for C^R_{ft} with wave function renormalization Z_R is the "sawtooth" function (for $a = 1$)

$$C^R_{ft}(t,p_1,p_2) = Z_R G_t(p_1,p_2), \quad (6)$$

for $t = 0, 2, \ldots, N_t - 2$, and

$$C^R_{ft}(t,p_1,p_2) = -\frac{Z_R}{2m_R}\Big[\exp(iB_0)\, G_{t+1}(p_1,p_2) - \exp(-iB_0)\, G_{t-1}(p_1,p_2)\Big], \quad (7)$$

for $t = 1, 3, \ldots, N_t - 1$, with anti-periodic boundary conditions. The function $G_t(p_1,p_2)$ is given by

$$\begin{aligned} G_t(p_1,p_2) \equiv N\big[&\cos(B_0N_t/2)\cosh(\mu_tN_t/2) \\ &\times \cos(B_0t^\star)\sinh(\mu_t t^\star) + \sin(B_0N_t/2)\sinh(\mu_tN_t/2) \\ &\times \sin(B_0t^\star)\cosh(\mu_t t^\star) + i\cos(B_0N_t/2)\cosh(\mu_tN_t/2) \\ &\times \sin(B_0t^\star)\sinh(\mu_t t^\star) - i\sin(B_0N_t/2)\sinh(\mu_tN_t/2) \\ &\times \cos(B_0t^\star)\cosh(\mu_t t^\star)\big], \end{aligned} \quad (8)$$

where $t^\star \equiv N_t/2 - t$,

$$N \equiv \frac{2m_R}{\sinh(2\mu_t)} \left[\cosh^2(\mu_t N_t/2) - \sin^2(B_0 N_t/2)\right]^{-1}, \quad (9)$$

and the dispersion relation

$$\sinh^2(\mu_t) \equiv m_R^2 + \lambda_R^2 \sin^2(p_1) + \lambda_R^2 \sin^2(p_2). \quad (10)$$

The expression for C_{ft}^R includes a constant "background field" $B_0 \equiv \langle\theta_0\rangle$ in C_{ft}^R, as $\langle\theta_0\rangle \neq 0$ in a finite volume. The background field B_0 is roughly bounded by $\pm\pi/N_t$ [21]. Note that the imaginary part of C_{ft}^R vanishes in the limit $B_0 \to 0$.

We also consider spatial correlations, to evaluate the effects of anisotropies. We define the spatial fermion correlator

$$C_{fx}(x, \omega, p_2) \equiv \sum_{t,y} \exp(-ip \cdot x)\, C_f(t, x, y), \quad (11)$$

for $\omega = 2\pi(n - 1/2)/N_t$ (due to the anti-periodic temporal boundary conditions), $n = -N_t/4, \ldots, N_t/4$, spaceslices $x = 0, \ldots, N_x - 1$, and summation over even lattice sites. The expression for C_{fx}^R can be inferred from C_{ft}^R. The function $G_x(\omega, p_2)$ is obtained from Eq. (8) by first exchanging $\sin \leftrightarrow \cos$, followed by the substitutions $t \to x$, $N_t \to N_x$, $\mu_t \to \mu_x$ and $B_0 \to 0$. These also apply to Eq. (7) and (9), in addition to $m_R \to m_R/\lambda_R$ in Eq. (7) and $m_R \to m_R/\lambda_R^2$ in Eq. (9). The dispersion relation is

$$\sinh^2(\mu_x) \equiv m_R^2/\lambda_R^2 + \sin^2(\omega + B_0)/\lambda_R^2 + \sin^2(p_2). \quad (12)$$

Unlike Eqs. (6) and (7), C_{fx}^R is real-valued and satisfies periodic boundary conditions.

In Fig. 1, we show λ_R as obtained from a chi-square fit of Eqs. (7) and (8) to LMC data. While Eq. (1) is gauge invariant, the fermion correlators C_{ft} and C_{fx} are not, and thus a gauge fixing condition is imposed on each configuration in order to obtain stable results. For C_{ft}, a correlated fit is performed for all t, p_1, p_2, and in the case of C_{fx} for all x, ω, p_2. The fitted parameters are m_R, λ_R, B_0 and Z_R. Our lattices have $N_t = N_x$, and the length of the "bulk" dimension (where only the photons propagate) is denoted N_b. We use the notation $N_x^3 \times N_b$, and simply N_x^4 when $N_b = N_t = N_x$. On the $28^3 \times 8$ lattice, LMC data is available for (inverse) lattice couplings $5.0 \leq \beta^{-1} \leq 15.0$, and for bare quasiparticle masses $0.0025 \leq m_0 \leq 0.020$, with slightly more restrictive data sets on the $32^3 \times 12$ and 32^4 lattices. We find that λ_R increases monotonically as a function of α_g from the non-interacting value of unity, with no appreciable differences between λ_R as obtained from C_{ft} and C_{fx}. We find the dependence on m_0 to be almost negligible. Finite size effects for λ_R are small, and the fitted values of B_0 agree closely with $\langle\theta_0\rangle$.

In Fig. 2, we show the physical quasiparticle mass m_R as a function of β and m_0, with emphasis on asymmetries between the temporal and spatial correlations, and on finite size effects. As Eq. (1) treats space and time asymmetrically, the spatial and temporal correlation lengths ξ may exhibit unequal critical scaling, such that $\xi_s \propto |\beta - \beta_c|^{-\nu_s}$ and $\xi_t \propto |\beta - \beta_c|^{-\nu_t}$.

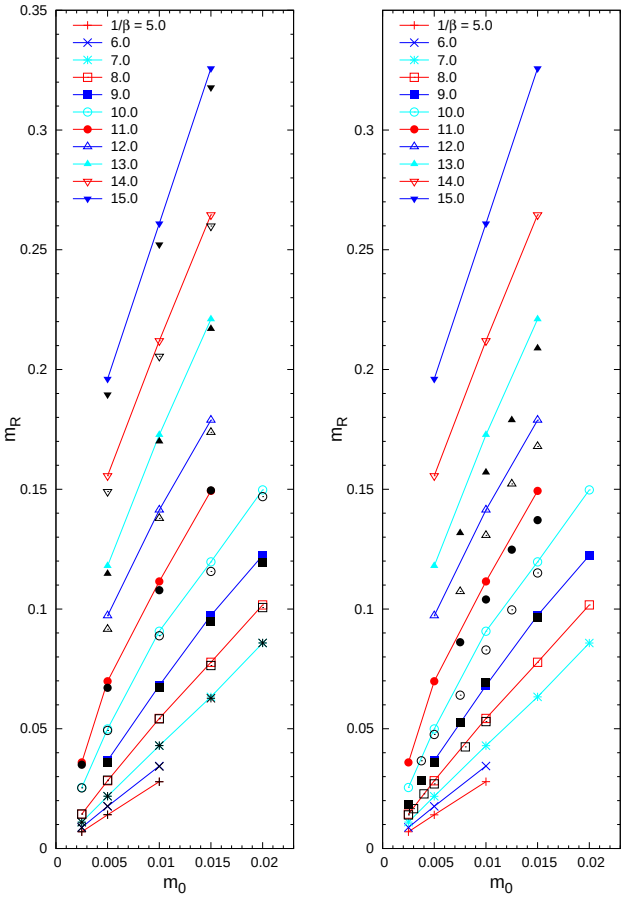

FIG. 2: Calculation of the physical quasiparticle mass m_R as a function of $\beta^{-1} = 4\pi\alpha_g$ and m_0 (for $a = 1$). Left panel: Calculation of m_R from temporal (colored connected symbols) and spatial (black unconnected symbols) correlations on a $28^3 \times 8$ lattice. Right panel: Calculation of m_R from temporal correlations on a $28^3 \times 8$ lattice (colored connected symbols) and on a $32^3 \times 12$ lattice (black unconnected symbols). All lines are intended as a guide to the eye, and statistical errors are comparable to the size of the symbols.

The dynamical critical exponent $z \equiv \nu_t/\nu_s$ is an important characteristic of a quantum critical point (QCP), and implies that the dispersion relation is modified to $E \propto p^z$. At large N_f, Ref. [6] predicted $z \simeq 0.8$ for graphene in the strong-coupling limit. However, arguments have also been put forward which indicate $z = 1$ for a QCP with $d < 4$ in theories with a long-range Coulomb interaction [27]. From Fig. 2, we find that the values of m_R obtained from C_{ft} and C_{fx} agree very closely for $\beta^{-1} \leq 11.0$, which is consistent with $z \simeq 1$. We also find no sign of non-linear dispersion. A more accurate analysis is possible following Ref. [12], in terms of the equation of state (EOS)

$$m_0 = A(\beta - \beta_c)\, m_R^{(\delta\cdot\beta_m - 1)/\nu_t} + B\, m_R^{\delta\cdot\beta_m/\nu_t}, \quad (13)$$

for m_R computed from C_{ft}, where δ and β_m are critical exponents characterizing the QCP at $\beta = \beta_c$. An analogous EOS with $\nu_t \to \nu_s$ can be given for m_R as obtained from

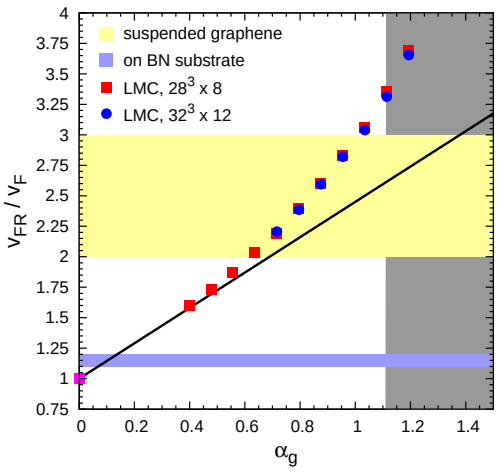

FIG. 3: Plot of $v_{FR}(\alpha_g)/v_F$ for asymmetry $(a/a_x)_R \simeq 1$. The critical velocity renormalization is $v_c \simeq 3.3$ at $\alpha_{gc} \simeq 1.1$, and the predicted insulating phase occurs for $\alpha_g > \alpha_{gc}$ (gray shaded area). We find a linear dependence of v_{FR}/v_F on α_g up to $\alpha_g \simeq 0.5$ (solid black line). Note that $v_{FR}(0)/v_F \equiv 1$. Horizontal bands indicate empirical data on v_{FR}/v_F from Ref. [7] (suspended graphene) and Ref. [8] (graphene on a BN substrate).

C_{fx}. We also find from Fig. 2 that finite size effects are under control for $\beta^{-1} \leq 9.0$, but not for smaller β (stronger coupling), especially in the region of the phase diagram where a dynamically generated gap exists, *i.e.* $\lim_{m_0 \to 0} m_R \neq 0$. In principle, Eq. (13) can be used to compute z and m_R in the limit $m_0 \to 0$, *i.e.* the gap in the quasiparticle spectrum. The lattice spacing asymmetry $(a/a_x)_R$ could then be inferred by measuring the gap in terms of temporal and spatial correlations. For reliable conclusions, such an EOS analysis should be combined with an extrapolation to infinite volume, similar to that of Ref. [22] for QED_4. For the present analysis, we note from Fig. 2 that the values of m_R computed from C_{ft} and C_{fx} differ by no more than $\simeq 10\%$ at the smallest values of β. Assuming this trend persists in the limits of infinite volume and vanishing m_0, we find $1.0 \leq (a/a_x)_R \leq 1.1$ over the range of α_g studied. In the absence of substantial indications for $(a/a_x)_R \neq 1$, we take λ_R as a measure of v_{FR}/v_F.

In Fig. 3, we summarize our LMC results for v_{FR}/v_F as a function of $\alpha_g \equiv 1/(4\pi\beta)$, and compare with available experimental data. We find that v_{FR} increases linearly with α_g from the non-interacting value v_F up to $\alpha_g \simeq 0.5$, above which the increase becomes more rapid. At the predicted critical coupling $\alpha_{gc} \simeq 1.1$, we find $v_c \equiv v_{FR}(\alpha_{gc})/v_F \simeq 3.3$ for the critical velocity renormalization. Since all of the empirical v_{FR}/v_F fall short of v_c, we find a plausible explanation for the non-observation of excitonic insulating phases in graphene monolayers. Nevertheless, the result of Ref. [7] is tantalizingly close to v_c, which suggests that further refinements in the quality of suspended graphene may suffice to trigger the excitonic instability. From Fig. 3, we find that $2 \leq v_{FR}/v_F \leq 3$ reported by Ref. [7] in suspended graphene corresponds to $\alpha_g \simeq 0.7 - 0.9$, although it should be kept in mind that α_g is an unrenormalized parameter. While the electron charge is believed [28] not to be renormalized, the calculation of e_R in graphene remains a challenge for LMC.

The recent study of the velocity renormalization in extrinsic graphene ($n \neq 0$) by Ref. [29] has predicted a dramatic breakdown of the quasiparticle picture, which should be observable in graphene on an SiO_2 substrate ($\alpha_g = 0.8$), and dominate the spectral properties in suspended graphene ($\alpha_g = 2.2$). While we find no breakdown of the description in terms of a renormalized quasiparticle propagator, our LMC data extends only to $\alpha_g \simeq 1.2$, thus we cannot at present determine whether the quasiparticle picture remains valid at larger couplings.

We thank Lars Fritz, Simon Hands and Gerrit Schierholz for instructive discussions, and Jan Bsaisou, Dean Lee and Ulf-G. Meißner for a careful reading of the manuscript. T. L. acknowledges financial support from the Helmholtz Association (contract VH-VI-417). This work was supported in part by an allocation of computing time from the Ohio Supercomputer Center (OSC).

[1] K. S. Novoselov, Science **306**, 666 (2004); K. S. Novoselov *et al.*, Proc. Natl. Acad. Sci. U.S.A. **102**, 10451 (2005); Nature (London) **438**, 197 (2005); A. K. Geim and K. S. Novoselov, Nature Mater. **6**, 183 (2007).
[2] A. H. Castro Neto, F. Guinea, N. M. R. Peres, K. S. Novoselov, and A. K. Geim, Rev. Mod. Phys. **81**, 109 (2009).
[3] V. N. Kotov, B. Uchoa, V. M. Pereira, F. Guinea, and A. H. Castro Neto, Rev. Mod. Phys. **84**, 1067 (2012).
[4] J. González, F. Guinea, and M. A. Vozmediano, Nucl. Phys. **B424**, 595 (1994).
[5] J. González, F. Guinea, and M. A. Vozmediano, Phys. Rev. B **59**, 2474(R) (1999); S. Das Sarma, E. H. Hwang, and W.-K. Tse, *ibid.* **75**, 121406(R) (2007); M. Polini, R. Asgari, Y. Barlas, T. Pereg-Barnea, and A. H. MacDonald, Solid State Commun. **143**, 58 (2007); M. S. Foster and I. L. Aleiner, Phys. Rev. B **77**, 195413 (2008); V. N. Kotov, B. Uchoa, and A. H. Castro Neto, *ibid.* **80**, 165424 (2009).
[6] D. T. Son, Phys. Rev. B **75**, 235423 (2007);
[7] D. C. Elias *et al.*, Nature Phys. **7**, 701 (2011).
[8] G. L. Yu *et al.*, Proc. Natl. Acad. Sci. U.S.A. **110**, 3285 (2013).
[9] D. A. Siegel *et al.*, Proc. Natl. Acad. Sci. U.S.A. **108**, 11365 (2011).
[10] E. V. Gorbar, V. P. Gusynin, V. A. Miransky, and I. A. Shovkovy Phys. Rev. B **66**, 045108 (2002); D. V. Khveshchenko and H. Leal, Nucl. Phys. **B687**, 323 (2004); D. V. Khveshchenko, J. Phys. Condens. Matter **21**, 075303 (2009); G.-Z. Liu, W. Li, and G. Cheng, Phys. Rev. B **79**, 205429(R) (2009); O. V. Gamayun, E. V. Gorbar, and V. P. Gusynin, *ibid.* **81**, 075429 (2010).
[11] T. DeGrand and C. DeTar, *Lattice Methods for Quantum Chromodynamics* (World Scientific, Singapore, 2006).
[12] S. J. Hands and C. G. Strouthos, Phys. Rev. B **78**, 165423 (2008); W. Armour, S. Hands, and C. Strouthos, *ibid.* **81**, 125105 (2010).
[13] J. E. Drut and T. A. Lähde, Phys. Rev. Lett. **102**, 026802 (2009); Phys. Rev. B **79**, 241405 (2009); *ibid.* **79**, 165425(R) (2009).
[14] E. Shintani and T. Onogi, arXiv:1203.1091 [hep-lat].

[15] S. Sorella and E. Tosatti, Europhys. Lett. **19**, 699 (1992); M. Paiva, R. T. Scalettar, W. Zheng, R. R. P. Singh, and J. Oitmaa, Phys. Rev. B **72**, 085123 (2005); Z. Y. Meng, T. C. Lang, S. Wessel, F. F. Assaad, and A. Muramatsu, Nature (London) **464**, 847 (2010).
[16] G. V. Semenoff, Phys. Rev. Lett. **53**, 2449 (1984).
[17] V. P. Gusynin, S. G. Sharapov, and J. P. Carbotte, Int. J. Mod. Phys. B **21**, 4611 (2007).
[18] J. Kogut and L. Susskind, Phys. Rev. D **11**, 395 (1975); L. Susskind, *ibid.* **16**, 3031 (1977); H. Kluberg-Stern, Nucl. Phys. **B220**, 447 (1983); C. Burden and A. N. Burkitt, Europhys. Lett. **3**, 545 (1987).
[19] E. Dagotto, J. B. Kogut, and A. Kocić, Phys. Rev. Lett. **62**, 1083 (1989); S. J. Hands, J. B. Kogut, and C. G. Strouthos, Nucl. Phys. **B645**, 321 (2002); S. J. Hands, J. B. Kogut, L. Scorzato, and C. G. Strouthos, Phys. Rev. B **70**, 104501 (2004).
[20] J. B. Kogut, E. Dagotto, and A. Kocić, Phys. Rev. Lett. **60**, 772 (1988); M. Göckeler *et al.*, *ibid.* **80**, 4119 (1998).
[21] M. Göckeler *et al.*, Nucl. Phys. **B371**, 713 (1992).
[22] M. Göckeler *et al.*, Nucl. Phys. **B487**, 313 (1997).
[23] L. Del Debbio, S. J. Hands, and J. C. Mehegan, Nucl. Phys. **B502**, 269 (1997); S. Christofi, S. J. Hands, and C. G. Strouthos, Phys. Rev. D **75**, 101701 (2007).
[24] S. Chandrasekharan and A. Li, Phys. Rev. Lett. **108**, 140404 (2012).
[25] H. J. Rothe, *Lattice Gauge Theories – An Introduction* (World Scientific, Singapore, 2005), 3rd ed.
[26] S. Duane, A. D. Kennedy, B. J. Pendleton, and D. Roweth, Phys. Lett. B **195**, 216 (1987); S. Gottlieb, W. Liu, D. Toussaint, R. L. Renken, and R. L. Sugar, Phys. Rev. D **35**, 2531 (1987).
[27] I. F. Herbut, Phys. Rev. Lett. **87**, 137004 (2001).
[28] J. Ye and S. Sachdev, Phys. Rev. Lett. **80**, 5409 (1998); I. F. Herbut, Phys. Rev. Lett. **97**, 146401 (2006).
[29] S. Das Sarma and E. H. Hwang, Phys. Rev. B **87**, 045425 (2013).